INTERNATIONAL JOURNAL OF AUTOMOTIVE AND MECHANICAL ENGINEERING (IJAME)
ISSN: 2229-8649 e-ISSN: 2180-1606
VOL. 19, ISSUE 2, 9709 – 9720
DOI: https://doi.org/10.15282/ijame.19.2.2022.07.0749

ORIGINAL ARTICLE

Process Parameters Optimisation and Numerical Simulation of Laser Beam Welded Butt Joints of Maraging Steel

I.Rama Pavan Kumar Varma[1], P.Rama Murty Raju[1], Ch.Srinivasa Rao[2] and S. Rajesh[1]

[1]Department of Mechanical Engineering, SRKR Engineering College, Bhimavaram, 534204 A.P, India
[2]University College of Engineering, Andhra University, Vishakhapatnam, 530003 A.P, India

ABSTRACT – Maraging steels are ultra-high strength iron nickel-based alloys which are used in military applications like rocket motor casings, missiles, and ship hulls. In the current work, maraging steels of 250 grade butt joints with 2 mm thickness are welded by using Nd:YAG laser. The experiments were designed and conducted using the L16 orthogonal array. Various welding parameters selected for the current work are laser power, welding speed, and focal position, whereas tensile strength, hardness and depth of penetration were considered as the output responses. The influence of process variables on weld bead morphology was analysed experimentally. The microstructure, mechanical characteristics and numerical analysis of the optimum joint were also investigated. Analysis of variance (ANOVA) was used to determine the effect of different variables on tensile strength and depth of penetration. According to the results, laser power and welding speed are essential factors for tensile strength. The depth of penetration is strongly influenced by welding speed, focal position, and laser power. In order to predict the weld bead, finite element analysis was performed on ABAQUS 3D finite element software. The results reveal that finite element simulation and experimental observations are matched.

ARTICLE HISTORY
Received: 25th Oct 2021
Revised: 21st May 2022
Accepted: 16th June 2022
Published: 28th June 2022

KEYWORDS
Maraging steels;
Laser beam welding;
Heat affected zone;
Microstructural analysis;
Finite element analysis

INTRODUCTION

Advances in the field of aerospace and defence are demanding increased utilisation of steels that possess ultra-high strength, toughness, high reliability, and good performance at a low weight of the material. Maraging steels are low carbon iron and Ni system with different fractions of Co, Mo, Ti and Al. Generally, these steels are given good strength through the ageing process where the substitutional elements like Ni, Ti and Mo are precipitated. Maraging steels have excellent compatibility to form very large structures as they can be easily weldable in the solution phase [1-3]. The peculiarity of maraging steel is its high strength, good fracture toughness and commendable weld ability at a very low carbon content [4]. The two solid-state processes called MAR-AGING (i.e. a martensitic transformation accompanied by ageing, are mainly responsible of the excellent mechanical properties of this material. It is also observed to enhance the strength of Ni-Co-Mo maraging steels by precipitation of intermetallic compounds.[5]. Shamantha et al. [6] found that during the ageing of welded maraging steels, hardening occurs. Laser beam welding (LBW) is a popular method for bonding different materials [7-9]. In recent times, it has been widely used for joining maraging steels with 18% Ni where welding defects can be kept to a minimum under an inert gas atmosphere. The main features of laser beam welding include very low heat input, deep penetration, little heat-affected zone, very tiny fusion zone and high flexibility. In the past, many researchers [10-13] studied the laser beam welding process. Numerous examinations have been done on the use of laser welding of different compounds, for example, Ti-6Al-4V titanium alloy and 18% Ni maraging steel [14]. Benyounis and Olabi [15] have stated that the influence of laser welding parameters on weld bead geometry can be eliminated by the laser butt welding of medium carbon steel. A mathematical model developed by Manonmani et al. [16] using RSM envisage the major effects of laser beam welding on the variables of weld bead geometry.

Prabakaran et al. [17] improved laser welding process parameters for austenitic stainless steel (AISI 316) and low carbon steel (AISI 1018) materials using Taguchi-based grey relational analysis. After post-weld heat treatment, the optimal welded joint displayed favourable mechanical properties, with a maximum tensile strength of 475.112 MPa at 960 °C. Subashini et al. [18] used a CO_2 laser and a pulsed MIG welding power source to investigate single-pass laser-MIG hybrid welding (LHW) of 10-mm-thick maraging steel plates. The focus of this research is to better understand the function of filler wire in the LHW process vs the ALW process. Fanton et al. [19] used LBW satisfactorily welded thin sheets to medium thick sheets of maraging steel, but thick sheets are hard to obtain an exceedingly low edge space and proper joint fit. Ahn et al. [20] studied LBW (4 kW) of maraging steel plate of thickness 2 mm at different laser power, defocusing distance and the welding speed. The study shows that the major welding defects are found to be as spatter and undercut at higher laser beam power, while inadequate penetration occurs at low power of the laser beam and at high welding speed. Kabir et al. [21] investigated the Ti64 alloy Nd: YAG, LBW at various welding speeds and the defocusing size. The effect of welding speed on surface properties, microstructure, defects, weld shape, hardness, and tensile properties while welding of 1 and 2 mm thick Ti64 plate using Nd: YAG laser was studied by Cao et al. [22]. However,

*CORRESPONDING AUTHOR | I.Rama Pavan Kumar Varma | ✉ pavan.srkr.varma @gmail.com

there is a substantial drop in ductility because of the appearance of aluminium oxide and the micro pores involved. Liu et al. [23] reported that heat treatment at 1050 ℃ for 15-60 minutes for a short time during post-weld could effectively restore the fusion zone and improve toughness.

Thermal stresses and microstructure transformation degrade the mechanical behaviour in FZ and HAZ of laser weldments. Reisgen et al. [24] have reported an optimisation method for continuous-wave CO_2 laser welding in terms of parameters like the laser power, speed of the welding and focusing position using RSM for the welding. They used varying thicknesses of DP600 steel of advanced high strength hand could obtain good geometry of weld bead, good mechanical properties, and formability in a cost-effective fabrication process. A report by Casalino et al. [25] demonstrates that usage of fibre laser welding may decrease contaminations by welding and oxidation on the adjacent surface when combined with 2 mm thick Ti64 alloy under different welding circumstances. It is carried out by providing a gas supply system of appropriate quantities of shielding gas. Here, an X and V shape bead were created by higher and lower heat input. In most cases of welding in maraging steels, the fracture happens mostly in the weld zone. The poor strength and toughness of the joints of the weld are normally assigned to the separation of the elements and to the formation of titanium and nitride inclusion. The cases where the heat treatment temperature goes above 820 ℃, the precipitates may have a greater impact on the mechanical properties of the maraging steels [26-29].

In Palanivel et al. [30], a 4 mm thick A588 grade K high strength low alloy (HSLA) connection was examined with the corresponding microstructural development utilising sophisticated methods. Derakhshan et al. [31] compared various laser-based welding processes with traditional fusion welding submerged arc welding (SAW). Finite element techniques have been developed to take into consideration the moving heat source, the transition of a solid-state phase, and the influence of fluid movement on the temperature distribution. Mehrpouya et al. [32] reported a thermal model in ABAQUS was created using the user material method to simulate the heat transfer and size of HAZ and FZ zones.

Existing literature showed a limited number of studies were carried out in maraging steel using laser welding. In the current research experimental study is performed on LBW of maraging steel in butt welding configuration by adopting the process variables such as laser power, welding speed and focal position to understand their influence on mechanical properties and depth of penetration. Further research was performed in order to determine the welding parameters using statistical analysis in order to improve welding efficiency. ANOVA is used to determine the contributing factor and their response to the output. However, this study is mainly focusing on bringing out a comprehensive understanding of the mechanical strength of the joints, i.e. tensile strength, depth of penetration, and microstructural characterisation of maraging steel occurred due to laser beam welding processes, and simulating the laser beam welding (LBW) process using ABAQUS, a 3D finite element software. The results reveal that finite element simulation and experimental observations are matched.

EXPERIMENTAL PROCEDURE AND METHODOLOGY

In this study, the base material used was maraging steel (250 grade), and butt weld experiments were performed on 115×100 mm sheets. The welding trials were conducted on a sheet of maraging steel having a thickness of 2 mm. The specimens were cut from each weldment in order to test the geometry of the weld bead. Acetone swabbing was used to rinse all the joints for protection from oil and oxide film contamination in the welding process. The 0.001 mm accuracy optical microscopy was utilised in order to measure the weld bead profile parameters such as the heat-affected zone upper width (HAZup), the fusion zone upper width (FZup) width and depth of penetration (DOP). Figure 1 represents the cut portion of the welded joints after machining in accordance with the ASTM E8 standards. The tensile test was done using a 100 kN universal testing machine. All tensile specimens were tested at room temperature with a speed of 0.00005-505 mm/min. Table 1 shows the chemical composition of the maraging steel.

Standard metallographic procedures were followed to appropriately section, mount and mechanically polish the specimens. After then, suitable etchants i.e. modified fry's reageant (of 37.5 ml water, 12ml Hcl,6ml HNO3 and $CuCl_2$ 0.25gm). Apart from this, 15% nital and 85% ethanol were used in the heat-affected zone (HAZ), fusion zone(FZ), and base material (BM) regions. An optical as well as a metallurgical microscope, namely, Olympus, was used for examining weldment microstructures of the welded joints of the different zones. A continuous wave Nd:YAG laser system was used for the entire welding procedure in this study. The initial joint position was set by fixing the plates with mechanical clamps. Mechanical clamps are used to position the plates securely in order to obtain the initial joint configuration. The selection of process parameters is very crucial to removing the defects during Nd-YAG laser welding. Taking all in consideration, the possible limits of the constraints were selected for the welding of the maraging steel. The characteristics of the welding process include laser power (LP), welding speed (WS) and focal location (FP). Argon was utilised as the shielding gas during the welding process and provided on one side at a steady flow rate of 50L/min. In the annealing heat treatment process, the welding joints are aged at 480 ℃ for 3 hours and then air is cooled in the joints for improvements in FZup, HAZup and DOP, then studied the changes in tensile strength and hardness. The soft martensite matrix of maraging steel is heated to 480 °C for three hours to generate a fine dispersion of hard precipitates. This method of precipitation hardening promotes strength by reducing dislocation movement caused by maraging steel precipitates. The experiments are designed according to Taguchi L_{16}orthogonal array. Table 2 shows the tabulations of each factor and their levels for maraging steel welding.

The joints are fabricated using a single pass welding procedure. Standard metallographic sample preparation was applied to the welds to observe their microstructure using an optical microscope. Microhardness test was done around the weld bead at the middle part of the entire welded joints with the load of a 300kgf Vickers intender microhardness unit

with a dwell time of 10 sec on the Mitsuzawa microhardness tester. The welded joints have been polished after sectioning by using an acceptable abrasive and diamond paste.

To simulate the moving heat element, user-defined subroutines were developed by using ABAQUS parametric design language and interfaced with ABAQUS. The size of the numerical model is the same as that of the specimen used in the experimental studies. Eight noded thermally coupled brick element is chosen for finite element modelling. The chosen mesh elements for the 3D finite element model are 8-node quadratic brick and 3D solid elements (C3D8T). A Gaussian conical 3D heat element model is used to perform a thermal analysis of laser beam welding of maraging steel 250. The predicted results showed good convergence when the model is meshed with 8572 hexagonal elements.

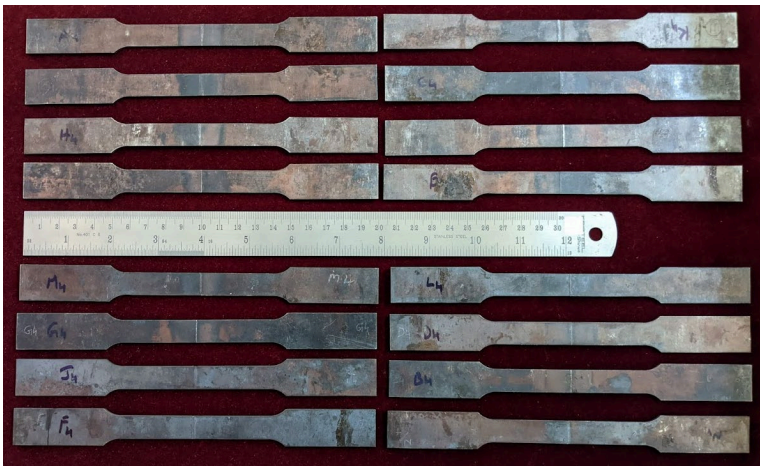

Figure 1. Tensile specimens for welded samples of maraging steels.

Table1. Chemical composition of maraging steel (MDN250).

Element	Ni	C	Co	Mo	Ti	Al	Mn	Fe
Wt %	18.9	0.02	8.1	4.9	0.4	0.15	0.04	Balance

Table 2. Welding parameters and its proportion.

Parameters	Notation	Units	Level 1	Level 2	Level 3	Level 4
Laser power	LP	kW	1	1.33	1.66	2
Welding speed	WS	m/min	0.6	1.2	1.8	2.4
Focal position	FP	mm	-1	0	1	2

RESULTS AND DISCUSSION

Tensile Strength and Depth of Penetration

In order to evaluate the mechanical characteristics of the joint, the tensile test was done at room temperatures. Figure 2 shows the broken tensile specimens, and it can be observed all the post-weld aged specimens getting fractured at FZ. Figure 3 represents a stress-strain curve for base material, maximum and minimum tensile strength specimens. The effect of process factors on joint tensile strength is depicted in Figure 4(a). Excessive penetration is found at lower welding speeds and lower laser power, resulting in underfill welding defects. In the case of lower laser power and higher welding speed, it can be noticed that incomplete penetration occurs. This might be the cause of the degradation of tensile strength and low penetration depth. We can observe that when the welding speed and focal position increases, tensile strength gradually decreases. The highest depth of penetration is observed at Level 1. The incomplete depth of penetration is obtained at Level 4. In Figure 4(b) we can observe that the laser power is the most influenced factor compared with other parameters. The higher value of laser power results in a higher depth of penetration because high laser power increases the power density, resulting in more depth of penetration, and it is clear that welding speed also greatly influences on the laser welded joint. For a higher speed of welding the penetration is less. The result shows that the DOP gets least affected by the focal position.

Figure 2. Fractured specimens.

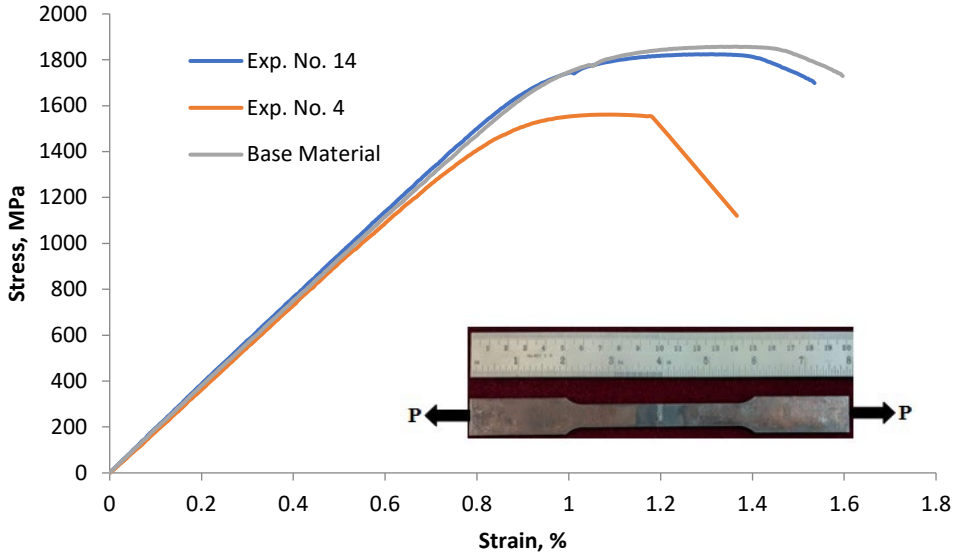

Figure 3. Tensile curves for Base material, sample 4 (min) and sample 14 (max) of laser beam welded specimens.

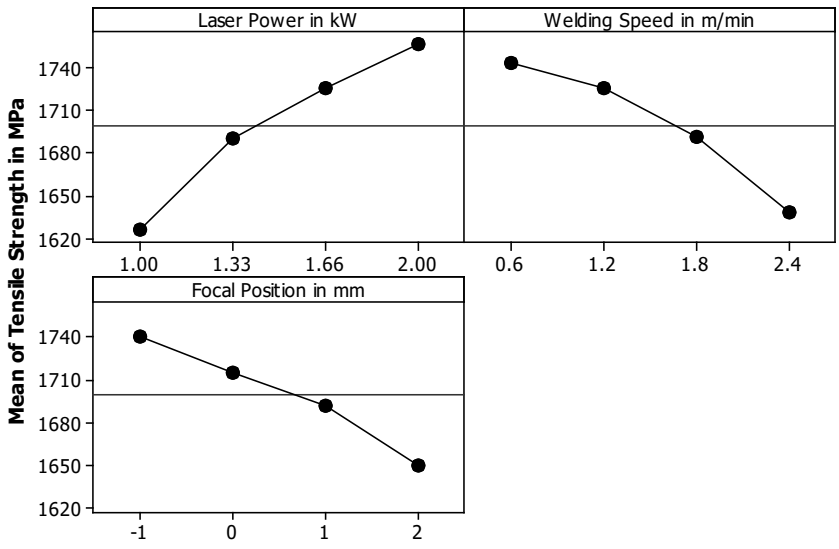

(a)

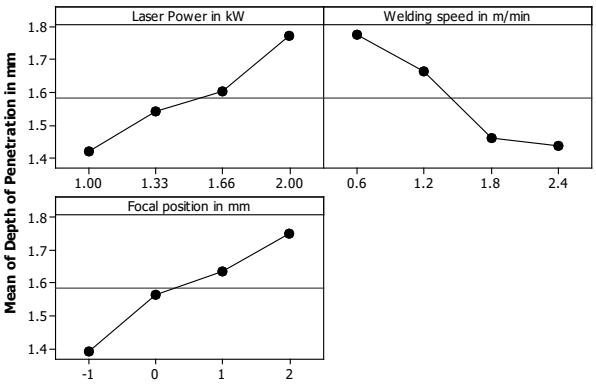

(b)

Figure 4. Main effect plot for (a) tensile strength, and (b) depth of penetration.

Table 3. Experimental observations with computed SNR for tensile strength and DOP of laser beam welding.

S. No.	LP (kW)	WS (m/min)	FP (mm)	Tensile strength (MPa)	D.O.P (mm)	TS-SNR	DOP-SNR
1	1	0.6	-1	1750.65	1.5098	64.864	3.57839
2	1	1.2	0	1653.54	1.4301	64.3683	3.10672
3	1	1.8	1	1590.21	1.3957	64.0291	2.89584
4	1	2.4	2	1510.23	1.3404	63.5809	2.54469
5	1.33	0.6	0	1750.98	1.6490	64.8656	4.34441
6	1.33	1.2	-1	1730.65	1.4525	64.7642	3.24232
7	1.33	1.8	2	1660.32	1.7250	64.4038	4.73578
8	1.33	2.4	1	1620.56	1.3490	64.1933	2.60024
9	1.66	0.6	1	1750.25	1.8433	64.862	5.31192
10	1.66	1.2	2	1708.63	1.8307	64.653	5.25234
11	1.66	1.8	-1	1750.98	1.1426	64.8656	1.15788
12	1.66	2.4	0	1690.54	1.5983	64.5605	4.07317
13	2	0.6	2	1720.67	2.0999	64.714	6.44397
14	2	1.2	1	1810.20	1.9513	65.1545	5.80648
15	2	1.8	0	1765.98	1.5773	64.9397	3.95829
16	2	2.4	-1	1730.54	1.4633	64.7636	3.30667

Microstructure

The optical microscopy image and their weld bead microstructures of the joints of maraging steels of 250 grades are shown in Figure 5(a). The microstructure of the base metal was significantly altered after post-weld heat treatment due to the development of intermetallic precipitates during ageing. The most frequent precipitates found in maraging steel are Ni3Mo and Ni3Ti [33]. The major microstructural change in the weld fusion area is the conversion of austenite to martensite during cooling at room temperature. FZ mostly comprises a cellular martensite structure. The regions adjacent to the fusion zone are three distinct bands, namely HAZ 1, HAZ 2, BMZ. The base material near the welding interface is heated during the welding process to high temperatures in the area of austenite, where significant grain growth occurs. FZ experiences either melting or solidification from all three zones. The microstructural properties of FZ vary with respect to the solidification nature of the welding pool, which in turn have a direct effect on the size and shape of the grains. This has an impact on the weld joint's mechanical strength. Weld bead profile of maraging steel comprises four different zones and is marked in Figure 5(a) as FZ, HAZ1, HAZ2 and BMZ. The FZ area that experiences peak temperatures is normally exhibited by the cellular grain structure shown in Figure 5(b). The HAZ1 shown in Figure 5(c) lies next to the fusion zone, which gets etched lightly like the base material. This zone is normally heated in the austenite region by weld thermal process but does not have a high grain growth rate at all. The welding interface of the parent material is heated to an elevated temperature during welding of the austenitic region, with the result that the grain growth increases significantly. The metal converts to martensite after cooling and inherits the size of the coarse austenite grain.

The HAZ2 shown in Figure 5(d) is a dark band area where the martensite stage encounters the hightest temperatures. Some reverted austenite formed in this zone in a martensitic substrate of a dark etched zone. This reverted austenite will not affect the strength and hardness. The dark etching area exhibits two-phase microstructures. The mixtures of martensite and austenite phase can be seen in the microscopic images of the fusion zones in the condition of ageing. BMZ, which is shown in Figure 5(e) is an unaffected parent metal during the welding cycle. Figure 5(f) represents the interface between FZ and HAZ. In the current work, there was a higher hardness found in HAZ2 due to coarsening of precipitates after post-weld heat treatments. Thus, this zone is found to be a soft zone, so it will not lower the tensile strength. It is further noticed that there is a lowering in the austenite reversion temperature as the austenite islands are formed along the boundaries of dendritic cells. When the FZ of maraging steel is completely converted to martensitic, due to its ductility behaviour, they

cannot be susceptible to cracking [34]. Under any of the experimental conditions mentioned here, such welded crackings are not observed in the welded specimens. It can be attributed mainly to the excellent crack resistance of the maraging steels.

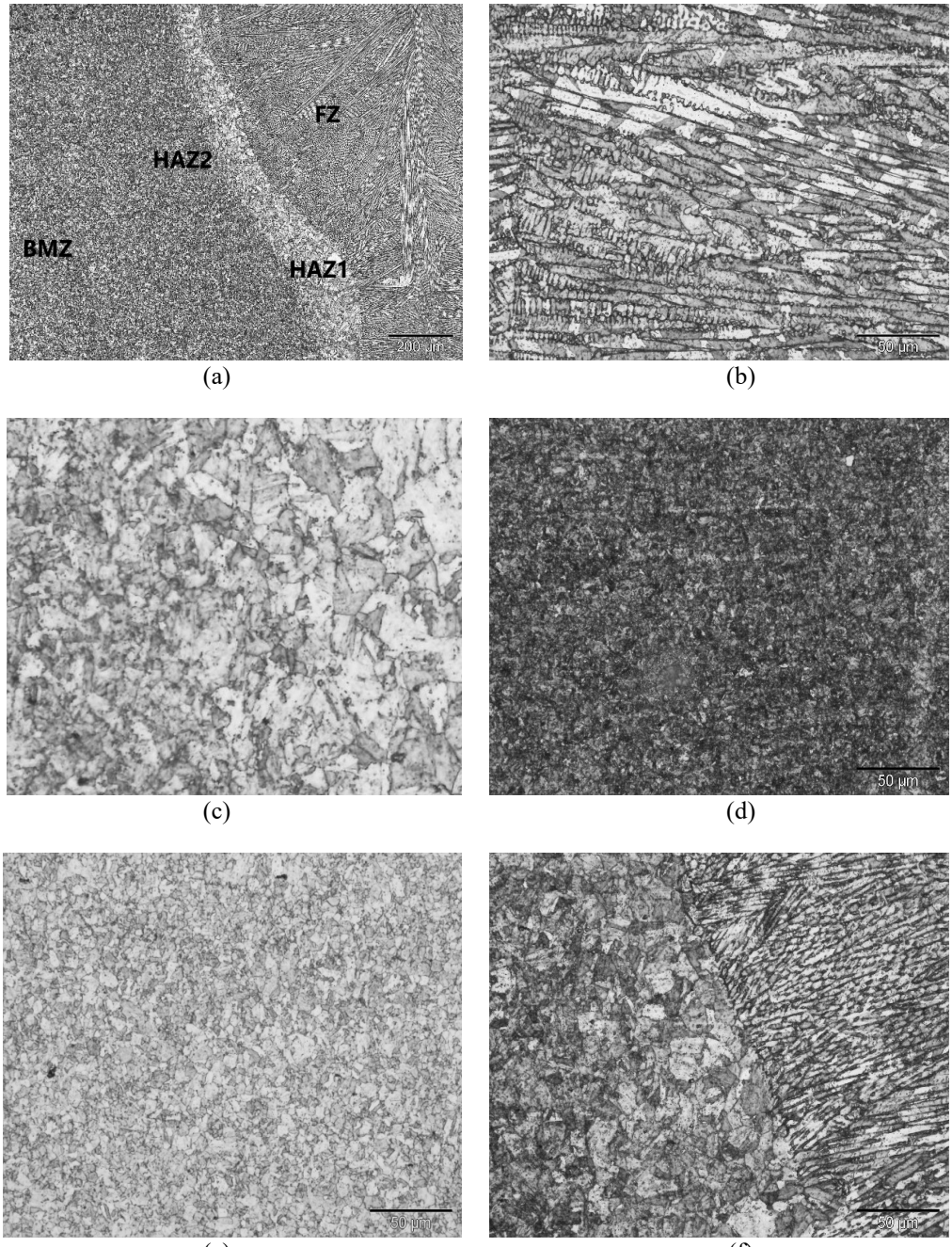

Figure 5. Micrographs of (a) bead profile, (b) fusion zone, (c) light etching region (HAZ1), (d) dark etching region (HAZ 2), (e) base metal zone, and (f) interface of FZ/HAZ.

Micro Hardness Distribution

A Vickers micro-hardness test machine has determined the hardness of the weld cross-section. Microhardness values measured on welded specimens are in aged conditions. The hardness profile for a 2 mm thick maraging steel joints was measured and reported here. The lowest hardness appeared at the centre of the FZ after welding and ageing treatment. As Ni is an austenite stabiliser, it lowers the austenite phase formation temperature of the Ni-enriched fusion zone, and thereby the segregation of alloying elements in the maraging steels, resulted in the accumulation of Ni in the weld zone. The ageing heat treatment results in a stable austenite phase (reverted austenite) and may not be converted into martensite phase effectively, which reduces the hardness of the fusion zone. This observation emphasises that the post-weld homogenisation treatment to laser beam welded maraging steels at sufficiently higher temperatures is required to acquire uniform mechanical properties of the weld joint. Moreover, significant greater hardness may be seen in HAZ due to the precipitation of various microstructures during the welding process. The highest hardness level in the HAZ is mainly because of the presence of martensitic structure as it possesses a high chilling rate in the FZ. The causes of increase of

hardness in the HAZ is because of finer grain structure and due to the formation of martensite structure. The high temperatures and cooling rate of LBW make the growth of martensite very conducive, which contributes to an improvement in the hardness of the HAZ area. The hardness of HAZ area can also be due to the formation of the martensite phase. From Figure 6, it can be found that the microhardness of HAZ is almost equal to the base metal and therefore, the figure also depicts higher microhardness for a faster welding speed is obtained. In Figure 6, when the input of heat decreases, the microhardness of FZ becomes lower than that of HAZ, that can be attributed to the formation of coarse grains. The microhardness of HAZ for all joints is observed to be much higher than as compared to the base metal. Unlike the earlier observations from literature, [35] where a significant variation in the hardness of HAZ was reported in the case of welding techniques where the laser was not used as a heating source. Such observations were largely attributed to the over-aging of the HAZ region during post-weld ageing treatments since the region has already undergone precipitation during the welding process itself, accompanied by the significantly higher prevailing temperatures over a fairly larger HAZ, unlike in laser-based welding processes.

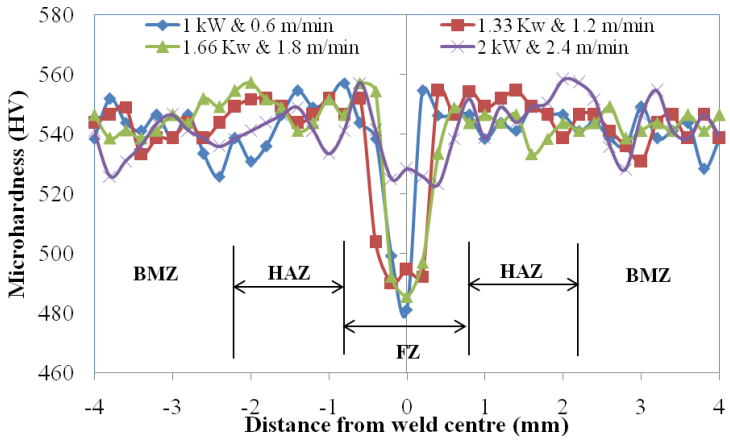

Figure 6. Hardness distribution maps.

Statistical Analysis

Statistical analysis of experimental data is performed in three phases. In the first step using multiple regression techniques, mathematical models for tensile strength and penetration depth with regard to welding parameters have been established. Subsequently, the Taguchi approach was employed for the L_{16} orthogonal array trials in the identification of optimum tensile strength and penetration depth values. Later, ANOVA was utilised for statistical analysis to assess the parameters that impact the tensile strength & penetration depth substantially. The analysis has been compared with the SNR response on the effect of each control element on tensile strength and penetration depth. The key parameters that influence the tensile strength and penetration depth for mean SNR values are shown in Figure 7. It is very clear from the figures that it can serve as an optimised testing condition for the control factors. The figure shows clearly how the SNR changes with the control factor level change. The greater SNR value was determined to have the optimum tensile strength. It can also be seen from Figure 7(a) and 7(b) that in tested samples, the optimal circumstances are LP4, WS1 and FP1 while the optimum conditions for the depth of penetration are LP4, WS1 and FP4 for primary control variables correspondingly. The following Eq. (1) and (2) were developed with an R2 of 89.4% and 84.5% for tensile strength and depth of penetration for using least square methods. The regression equations are given by:

$$\text{Tensile strength} = 1610 + 128 \text{ laser power} - 58.2 \text{ welding speed} - 29.5 \text{ focal position}$$
$$S = 27.7778 \quad \text{R-Sq} = 89.4\% \quad \text{R-Sq(adj)} = 86.8\% \tag{1}$$

$$\text{D.O.P} = 1.33 + 0.337 \text{ laser power} - 0.203 \text{ welding speed} + 0.114 \text{ focal position}$$
$$S = 0.111468 \quad \text{R-Sq} = 84.5\% \quad \text{R-Sq(adj)} = 80.6\% \tag{2}$$

where S represents the standard deviation of the distance between data values and fitted value, R-Sq represents the coefficient of determination, and R-Sq(adj) represents adjusted R-square.

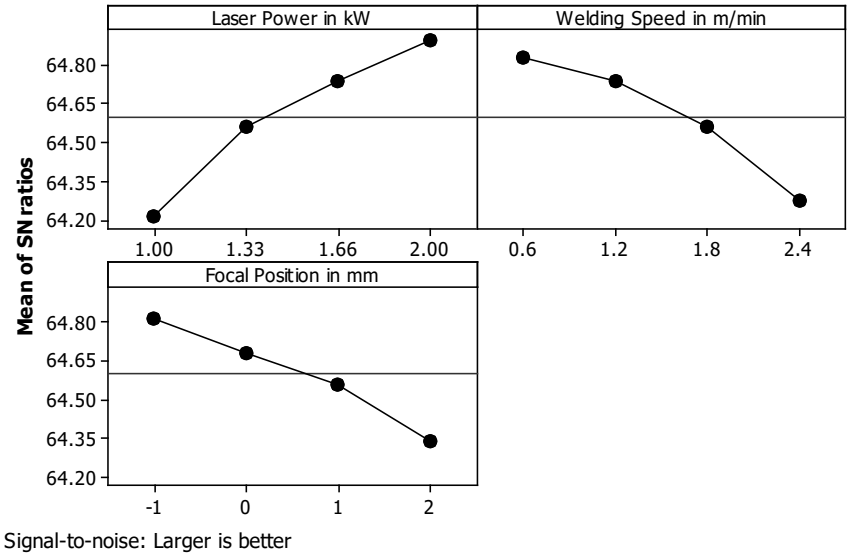

(a)

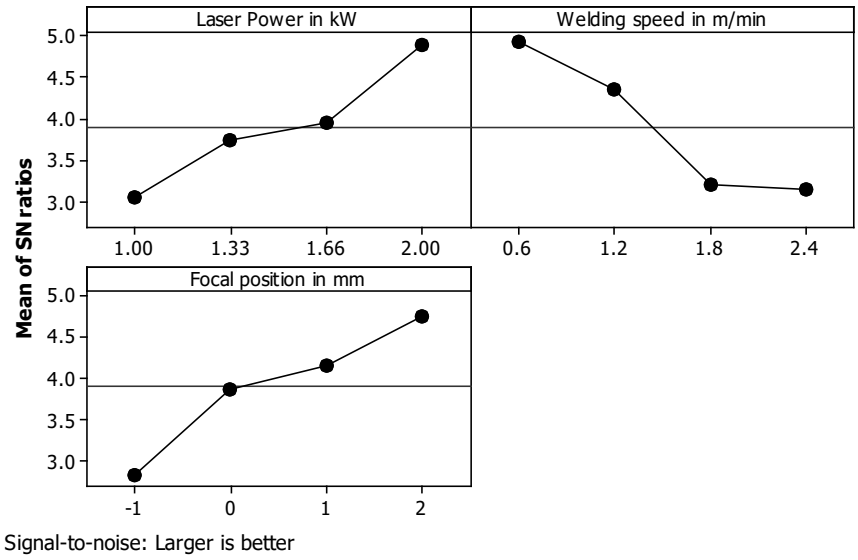

(b)

Figure 7. Main effect plots for SNR means of (a) tensile strength and (b) depth of penetration.

To study the parameters which substantially influence the quality, ANOVA data was done on the variables like laser power, welding speed and focal position. Further, in order to analyse the parameters which have an inevitable influence on response variables, the Fisher's F-test was also carried out. The results of ANOVA for Tensile strength and depth of penetration of laser beam welding are shown in Table 4 and Table 5. From the analysis of Table 4, it can be observed that laser power (43.04%) and welding speed (29.47%) influence the tensile strength, whereas the focal position had less influence (20.35%). Especially the laser power has a significant effect when compared to other factors. Table 5 shows that welding speed (30.98%), and focal position (27.18%) influences the depth of penetration, whereas the laser power (26.28 %) had less influence on the depth of penetration. These factors have physical significance only when its role is smaller than the relevant error. The results of ANOVA (Table 4 and Table 5) show that the error percentage is approximately 7.12% and 15.5% for the Tensile strength and the depth of penetration, respectively. As a result, this study concludes that laser power and welding speed have a considerable influence on tensile strength, whereas welding speed and focus position have a substantial effect on depth of penetration.

Table 4. Results of the ANOVA for Tensile strength for laser beam welding.

Predictor	SS	DF	Variance	F-calculated	% Contribution
Laser power	37607	3	12536	12.09	43.0492
Welding speed	25751	3	8584	8.28	29.4775
Focal position	17780	3	5927	5.72	20.3530
Error	6220	6	1037		7.1201
Total	87358	15			

Table 5. Results of the ANOVA for Depth of penetration for laser beam welding.

Predictor	SS	DF	Variance	F-calculated	% Contribution
Laser power	0.25220	3	0.08406	3.38269	26.2861
Welding speed	0.29730	3	0.09910	3.98792	30.9868
Focal position	0.26084	3	0.08694	3.49859	27.1866
Error	0.14910	6	0.02485		15.5403
Total	0.95944	15			

FINITE ELEMENT ANALYSIS

In order to predict the weld bead geometry, the finite element analysis was used to perform 3-D coupled thermo-mechanical analysis using a particular numerical software for the weld simulation, ABAQUS. Parametric studies have been carried out for laser power of 2 kW and welding speed of 600 mm/min. Figure 8(a) presents the weld bead geometry. The laser power of 2 kW and decreased welding speed of 600 mm/min increased the peak temperature (1487 °C) and weld profile formed into a cone shape with complete penetration weld bead, a small HAZ, and a maximum temperature which is shown in Figure 8(a). In order to compare the weld bead profile at optimal values, numerical simulation is performed for the experimental number 13 which is given in Table 3. From Figure 8(b), it can be noticed that for the laser power (2 kW), with a welding speed of 600 mm/min, the penetration depth is maximum with the formation of a keyhole and undercut. The results reveal that the depth of penetration increases by increasing laser power with lower welding speed. It confirms the heat transfer from top to bottom. Figure 8(c) shows the micrograph of laser beam welded joint.

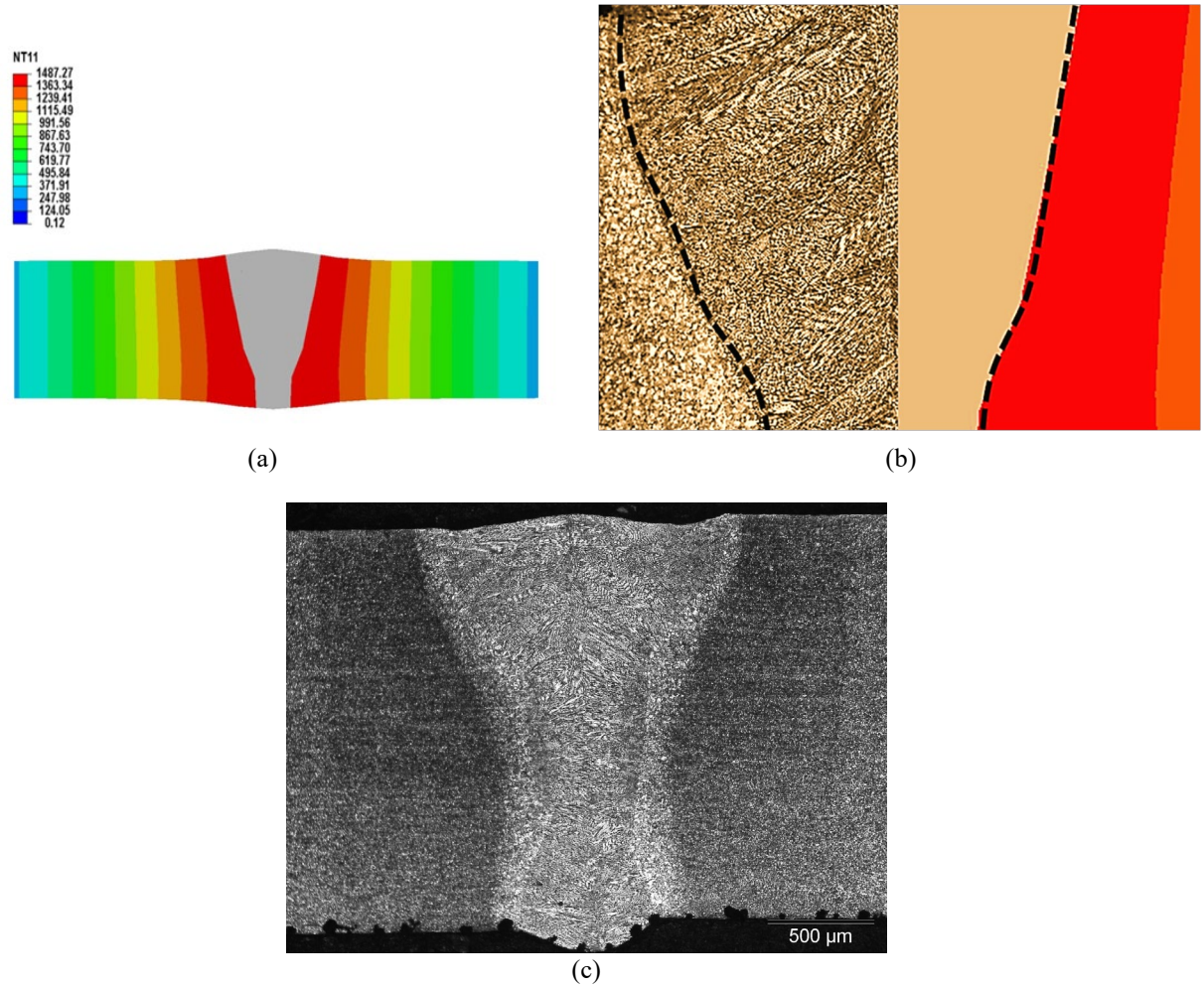

(a) (b)

(c)

Figure 8. (a) Weld bead geometry at laser power and welding speed of 2 kW and 600 mm/min obtained using ABAQUS. (b) Comparison with experimental and simulation results. (c) Micrograph of laser beam welded joint at 2 kW and a welding speed of 600 mm/min.

Temperature Distribution, Residual stresses, and Deformation

Welding residual stresses are caused by differential thermal expansion and contraction of the weld metal and parent material. Residual stress levels near the weld can be very high, up to material yield strength magnitude. To reduce the stress concentration, efforts have been made to achieve a favourable weld bead shape by welding process design and process control. The melting of the metal is used as part of the absorbed energy. The heat conduction is the primary mode

of heat transfer at the initial stage. At the intermediate point, the friction causes the free surface of the welding pool to deform. The temperature variation on the sample during the welding process for one of the laser conditions, i.e., 2 kW, 600 mm/min, and 2 mm, is shown in Figure 9. From Figure 9(a), it can be clearly observed that maximum temperature occurs in the vicinity of the laser beam and the arc gets stabilised at the centre of the plate at a temperature reaching 1487 °C, which indicates that the cooling temperature zone of the specimen is away from the heat source. Residual stresses developed were also predicted because of thermal input during welding. The deformation due to the welding process is primarily due to developed residual stresses. The von Mises stress distribution predicted at the mid-section of the plate and also after completion of the cooling period are presented. Figure 9(b), 9(c), and 9(d) present the von-Mises stress distribution at the mid-section of the plate, von Mises stress distribution after complete cooling and deformation corresponding to the complete cooling period, respectively. The magnitude of von Mises stress is 1140 MPa, and the value corresponding to complete cooling is 960 MPa. Following the cooling phase, the thermal deformation is calculated using the original requirements of maraging steel. According to the data, the largest distortion occurred at 0.3 mm and the least deformation occurred at 0.12 mm. The largest distortion of the maraging steel plate is found to occur at FZ and the minimum deformation at HAZ.

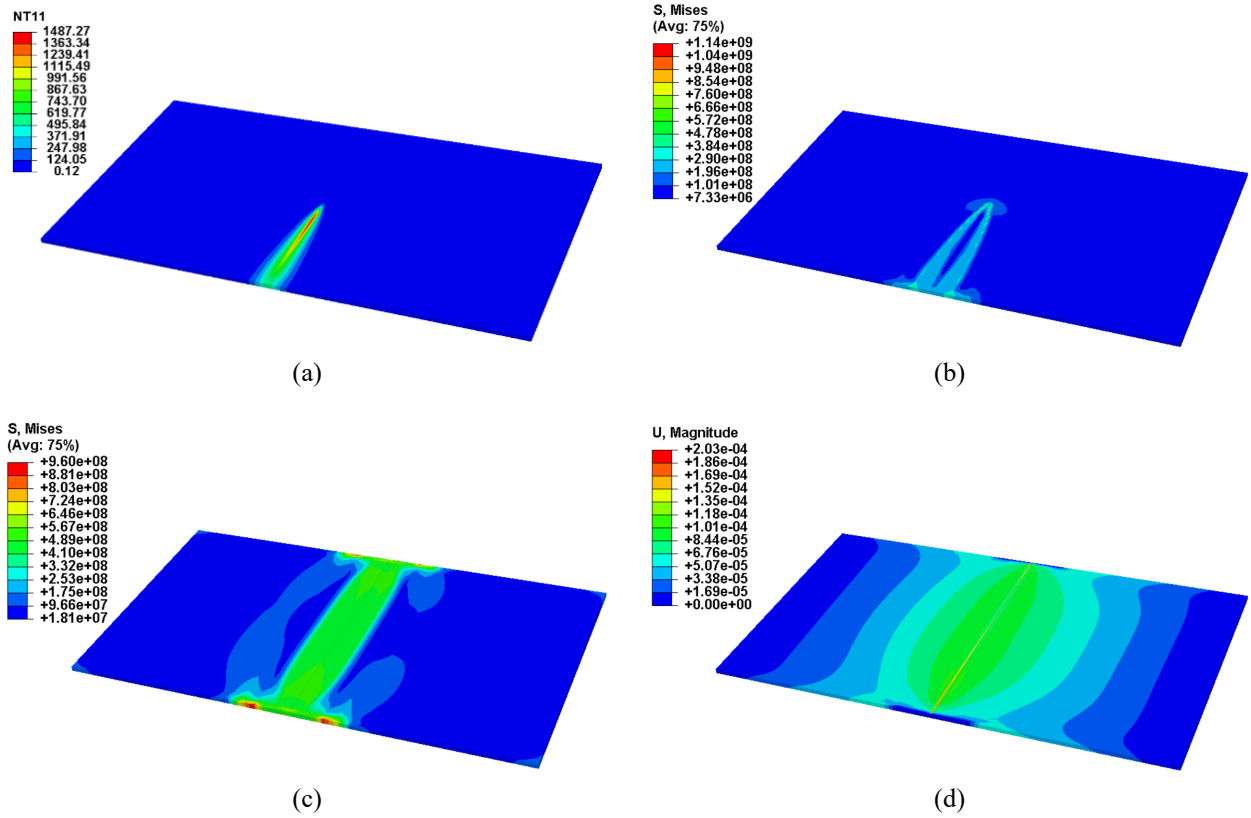

Figure 9. (a) Temperature distribution at maximum laser beam condition. (b) von Mises stress distribution at mid-section of plate; (c)von Mises stress distribution at the completion of cooling period (d) Deformation at the completion of cooling period.

CONCLUSION

The effect of parameters of weld on the tensile strength, hardness and penetration depth in the welding using laser beam on a 2mm thick maraging steel alloy in butt welding configuration performed using Nd:YAG laser at different welding conditions. Moreover, a statistical analysis is also performed to establish mathematical models to identify the optimal levels, most significant parameters of the weld and its contribution in responses to the output. In addition to it, a finite element analysis using ABAQUS was performed at optimal values to predict the weld bead geometry. From this investigation the following conclusion can be drawn:

i. Laser power (LP), welding speed (WS) and focal position (FP) are the main parameters which influence tensile strength and DOP.
ii. The maraging steel welded joints produced by using process parameters like laser power of 2 kW, welding speed of 1.2 m/min and focal position of 1 mm had achieved the highest tensile strength, which is almost equal to the tensile strength of the base material.
iii. From the examination of the microstructure of welded steel geometry, the main martensitic phase in the FZ and adjacent HAZ is detected. In HAZ, maximal hardness is observed due to the presence of martensitic structure.
iv. Based on the ANOVA results, The Laser power (43.04%) and welding speed (29.47%) influence the tensile strength, whereas the focal position has less influence (20.35%). It can be depicted that welding speed (30.98%),

and focal position (27.18%) influenced the depth of penetration, whereas the laser power (26.28%) has less influence on the depth of penetration.

v. From FE analysis, it was found that for the laser power (2 kW), with a welding speed of (600 mm/min), the depth of penetration is maximum, which indicates the heat transfer takes place from top to bottom.

vi. The width and morphology of the weld formed by numerical simulation are similar to experimental results.

ACKNOWLEDGEMENT

We thank the Director, Defence Research and Development Laboratory (DRDL), Kanchan Bagh, Hyderabad for providing laser beam welding and testing facilities for experimentation during the research work.

REFERENCES

[1] K. Li, J. Shan, C. Wang and Z.Tian, "The role of copper in microstructures and mechanical properties of laser welded Fe-19Ni-3Mo-1.5Ti maraging steel joint," *Mater. Sci. Eng. A*., vol. 681, pp.41-49, 2017. https://doi.org/10.1016/j.msea.2016.10.039.

[2] F. F. Conde *et al.*, "Effect of the as-built microstructure on the martensite to austenite transformation in a 18Ni maraging steel after laser-based powder bed fusion." *Addit. Manuf.*, vol. 46, 102122, 2021.https://doi.org/10.1016/j.addma.2021.102122.

[3] F. F. Conde *et al.*, "Austenite reversion kinetics and stability during tempering of an additively manufactured maraging 300 steel." *Addit. Manuf.,* vol. 29, 100804, 2019. https://doi.org/10.1016/j.addma.2019.100804.

[4] N. Sivagurumanikandan, S.Saravanan, G.S. Raju and K.Raghukandan, "Prediction and optimisation of process parameters to enhance the tensile strength of Nd: YAG laser welded super duplex stainless steel," *Optik.,* vol.157, pp.833-840, 2018. http://doi.org/10.1016/j.ijleo.2017.11.146.

[5] M. Ahmed, K. Hasnain, I. Nasim and H. Ayub, "Magnetic properties of maraging steels in relation to nickel concentration." *Metall. Mater. Trans. A.,* vol. 26, no. 7, pp. 1869-1876, 1995, https://doi.org/10.1007/BF02670774.

[6] C.R. Shamantha *et al.* "Microstructural changes during welding and subsequent heat treatment of 18Ni (250-grade) maraging steel." *Mater. Sci. Eng.,* vol. 287, no. 1, pp. 43-51, 2000, https://doi.org/10.1016/S0921-5093(00)00838-8.

[7] J. P. Oliveira *et al.*,"Dissimilar laser welding of a CoCrFeMnNi high entropy alloy to 316 stainless steel." *Scripta Materialia*, vol. *206*, pp. 114219. 2022. https://doi.org/10.1016/j.scriptamat.2021.114219.

[8] J. P. Oliveira *et al.*, "Laser welding of H-phase strengthened Ni-rich NiTi-20Zr high temperature shape memory alloy." *Mater. Des.,* vol. 202, pp.109533, 2021. https://doi.org/10.1016/j.matdes.2021.109533.

[9] W. Ke *et al.*, "Modeling and numerical study of keyhole-induced porosity formation in laser beam oscillating welding of 5A06 aluminum alloy." *Opt. Laser Technol.*, vol. 133, pp. 106540, 2021. https://doi.org/10.1016/j.optlastec.2020.106540

[10] A.E. Odermatt *et al.*, "Effect of laser beam welding on microstructure, tensile strength and fatigue behaviour of duplex stainless steel 2205." *J. Manuf. Process.*, vol. 72 pp. 148-158, 2021. https://doi.org/10.1016/j.jmapro.2021.10.020

[11] L. Subashini *et al.*, "Single pass laser-arc hybrid welding of maraging steel thick sections." *Mater. Manuf. Process.*, vol. 31, no. 16, pp. 2186-2198, 2016. https://doi.org/10.1080/10426914.2016.1221099.

[12] P.Pankaj, A.Tiwari, R.Bhadra and P.Biswas, "Experimental investigation on CO2 laser butt welding of AISI 304 stainless steel and mild steel thin sheets," *Opt. Laser. Technol.,* vol. 119, pp.105633, 2019, http://doi.org/10.1016/j.optlastec.2019.105633.

[13] MNM Salleh *et al.*, "Weld geometry investigation on dissimilar boron steel laser welded for TWB application." *Int. J. Automot. Mech. Eng.,* vol. 16, no. 4, pp. 7364-7374, 2019, https://doi.org/10.15282/ijame.16.4.2019.12.0546.

[14] M. Yu, F.Y. Meng, C. Liang and J. An. "Method for evaluating yield strength of laser weldments of maraging steels using hardness test." *Mater. Sci. Technol.,* vol. 29, no. 11, pp. 1317-132, 2013, https://doi.org/10.1179/1743284713Y.0000000275.

[15] K.Y. Benyounis, A.G. Olabi and M.S.J. Hashmi. "Effect of laser welding parameters on the heat input and weld-bead profile." *J. Mater Process Technol.,* vol. 164, pp. 978-985, 2005, https://doi.org/10.1016/j.jmatprotec.2005.02.060

[16] K. Manonmani K, Murugan N, Buvanasekaran G. "Effects of process parameters on the bead geometry of laser beam butt-welded stainless-steel sheets." *Int. J. Adv. Manuf. Technol*., vol. 32, no. 11, pp. 1125–1133, 2007, http://dx.doi.org/10.1007/s00170-006-0432-7

[17] M.P. Prabakaran and G.R. Kannan. "Optimisation of laser welding process parameters in dissimilar joint of stainlesssteel AISI316/AISI1018 low carbon steel to attain the maximum level of mechanical prpperties through PWHT." *Opt. Laser. Technol.,* vol. 112, pp.314-322, 2019, http://doi.org/10.1016/j.optlastec.2018.11.035

[18] L. Subashini, K.P. Prabhakar, S. Ghosh and G. padmanabham. "Comparision of laser-MIG hybrid and autogenous laser welding of m250 maraging steel thick sctions understanding the role of filler wire addition." *Int. J. Adv. Manuf. Tech.,* vol. 107(3), pp. 1581–1594, 2020, https://doi.org/10.1007/s000170-020-05113-3

[19] L. Fanton, A.J. Abdalla and M.S.F Lima. "Heat treatment and Yb-fiber Laser welding of a maraging steel." *Weld J.,* vol. 93, pp. 362-368, 2014.

[20] J. Ahn, L. Chen, C.M. Davies and JP Dear. "Parametric optimisation and microstructural analysis on high power Yb-fibre laser welding of Ti–6Al–4V." *Opt. Lasers. Eng.,* vol. 86, pp. 156–171, 2016, https://doi.org/10.1016/j.optlaseng.2016.06.002.

[21] A.S.H. Kabir *et al.,* "Effect of welding speed and defocusing distance on the quality of laser welded Ti-6Al-4V." *Lasers Manuf. Mater. Process.,* pp. 2787-2797, 2010.

[22] X. Cao and M. Jahazi. "Effect of welding speed on butt joint quality of Ti-6Al-4V alloy welded using a high-power Nd:YAG laser." *Opt. Lasers. Eng.,* vol. 47, no.11, pp. 1231-1241, 2009, https://doi.org/10.1016/j.optlaseng.2009.05.010

[23] H. Liu, X. Lu and X. Jin. "Phase transformation and mechanical properties in laser continuous heat treatment welds." *Mater. Des.,* vol. 32, no. 4, pp. 2269-2276, 2011, https://doi.org/10.1016/j.matdes.2010.11.016.

[24] U. Reisgen, M. Schleser, O. Markov, and E. Ahmed. "Optimisation of laser welding of DP/TRIP steel sheets using statistical approach." *Opt. Laser. Technol*., vol. 44, no. 1, pp. 255–262, 2012, https://doi.org/10.1016/j.optlastec.2011.06.028.

[25] G. Casalino, M. Mortello, and S.L. Campanelli. "Ytterbium fiber laser welding of Ti6Al4V alloy." *J. Manuf. Process.,* vol. 20, pp. 250–256, 2015, https://doi.org/10.1016/j.jmapro.2015.07.003.

[26] MNM Salleh *et al.*, "Weld geometry investigation on dissimilar boron steel laser welded for TWB application." *Int. J. Automot. Mech. Eng.,* vol. 16, no. 4, pp. 7364-7374, 2019, https://doi.org/10.15282/ijame.16.4.2019.12.0546.

[27] J. Tian *et al.*, "Effect of deformation on precipitation hardening behaviour of a maraging steel in the aging process," *Mater Charact.,* pp. 155, 2019 109827.http://doi.org/1016/j.matchar.2019.109827

[28] K. Li, J. Shan, C. Wang, and Z. Tian, "Influence of aging temperature on strength and toughness of laser-welded T-250 maraging steel joint." *Mater. Sci. Eng. A.*, vol. 669 pp. 58-65, 2016, https://doi.org/10.1016/j.msea.2016.05.043

[29] K. Li, J. Shan, C. Wang and Z. Tian, "Effect of post-weld heat treatments on strength and toughness behaviour of T-250 maraging steel welded by laser beam." *Mater. Sci. Eng. A.,* vol. 663, pp. 157-165, 2016, https://doi.org/10.1016/j.msea.2016.03.082.

[30] R. Palanivel, I. Dinaharan and R.F. Laubscher. "Microstructure and mechanical behaviour of Nd: YAG laser beam welded high strength low alloy steel joints." *Optik.,* vol. 208, pp. 164050, 2020, https://doi.org/10.1016/j.ijleo.2019.164050.

[31] E.D. Derakhshan, N. Yazdian, B. Craft, S. Smith and R. Kovacevic. "Numerical simulation and experimental validation of residual stress and welding distortion induced by laser-based welding processes of thin structural steel plates in butt joint configuration." *Opt. Laser. Technol.,* vol. 104, pp. 170-182, 2018, https://doi.org/10.1016/j.optlastec.2018.02.026.

[32] M. Mehrpouya, A. Gisario, H. Huang, A. Rahimzadeh and M. Elahinia. "Numerical study for prediction of optimum operational parameters in laser welding of NiTi alloy." *Opt. Laser. Technol.,* vol. 118, pp. 159-169, 2019, https://doi.org/10.1016/j.optlastec.2019.05.010.

[33] L. Kucerova, B. Karolina, S. Jenicek, and I. Chena, "Effect of solution annealing and precipitation hardening at 250 °C–550 °C on microstructure and mechanical properties of additively manufactured 1.2709 maraging steel." *Mater. Sci. Eng. A., vol.* 814 pp.141195, 2021, https://doi.org/10.1016/j.msea.2021.141195

[34] N. Kenyon, "Effect of austenite on the toughness of maraging steel welds," *Weld J.,* vol.47, no.5, pp. 193-198, 1968.

[35] X. Zhan *et al.*, "Investigation on parameter optimisation for laser welded butt joint of TA15 alloy." *Int. J. Adv. Manuf. Technol*., vol. 84, pp. 2697-2706, 2016, doi:10.1007/s00170-015-7900-x.